4. Katz, T. J. Syntheses of functionalized and aggregating helical conjugated molecules. *Angew. Chem. Int. Edn Engl.* **39,** 1921–1923 (2000).
5. Nelson, J. C., Saven, J. G., Moore, J. S. & Wolynes, P. G. Solvophobically driven folding of nonbiological oligomers. *Science* **277,** 1793–1796 (1997).
6. Hirschberg, J. H. K. K. *et al.* Helical self-assembled polymers from cooperative stacking of hydrogen-bonded pairs. *Nature* **407,** 167–170 (2000).
7. Berl, V., Huc, I., Khoury, R. G., Krische, M. J. & Lehn, J.-M. Interconversion of single and double helices formed from synthetic molecular strands. *Nature* **407,** 720–723 (2000).
8. Kirshenbaum, K., Zuckermann, R. N. & Dill, K. A. Designing polymers that mimic biomolecules. *Curr. Opin. Struct. Biol.* **9,** 530–535 (1999).
9. Stigers, K. D., Soth, M. J. & Nowick, J. S. Designed molecules that fold to mimic protein secondary structures. *Curr. Opin. Chem. Biol.* **3,** 714–723 (1999).
10. Lehn, J.-M. & Eliseev, A. V. Dynamic combinatorial chemistry. *Science* **291,** 2331–2332 (2001).
11. Lehn, J.-M. Dynamic combinatorial chemistry and virtual combinatorial libraries. *Chem. Eur. J.* **5,** 2455–2463 (1999).
12. Huc, I. & Lehn, J.-M. Virtual combinatorial libraries: Dynamic generation of molecular and supramolecular diversity by self-assembly. *Proc. Natl Acad. Sci. USA* **94,** 2106–2110 (1997).
13. Moore, J. S. & Zimmerman, N. W. "Masterpiece" copolymer sequences by targeted equilibrium-shifting. *Org. Lett.* **2,** 915–918 (2000).
14. Woodward, R. B., Sondheimer, F., Taub, D., Heusler, K. & McLarmore, W. M. The total synthesis of steroids. *J. Am. Chem. Soc.* **74,** 4223–4251 (1952).
15. Trost, B. M. The atom economy—A search for synthetic efficiency. *Science* **254,** 1471–1477 (1991).
16. Tóth, G., Pintér, I. & Messmer, A. Mechanism of the exchange reaction of aromatic Schiff bases. *Tetrahedr. Lett.* **15,** 735–738 (1974).
17. Prince, R. B., Saven, J. G., Wolynes, P. G. & Moore, J. S. Cooperative conformational transitions in phenylene ethylnylene oligomers: Chain-length dependence. *J. Am. Chem. Soc.* **121,** 3114–3121 (1999).
18. Pace, C. N., Shirley, B. A. & Thomson, J. A. in *Protein Structure: A Practical Approach* (ed. Creighton, T. E.) 311–330 (IRL, New York, 1989).
19. Goodman, M., Verdini, A. S., Toniolo, C., Phillips, W. D. & Bovey, F. A. Sensitive criteria for the critical size for helix formation in oligopeptides. *Proc. Natl Acad. Sci. USA* **64,** 444–450 (1969).
20. Zhang, J., Pesak, D. J., Ludwick, J. L. & Moore, J. S. Geometrically-controlled and site-specifically-functionalized phenylacetylene macrocycles. *J. Am. Chem. Soc.* **116,** 4227–4239 (1994).

Supplementary Information accompanies the paper on *Nature*'s website (http://www.nature.com).

Acknowledgements

We thank C. F. Zukoski and A. Y. Mirarefi for discussions and comments on light-scattering experiments. This work was supported by the National Science Foundation and the US Department of Energy, Division of Materials Sciences, through the Frederick Seitz Materials Research Laboratory at the University of Illinois at Urbana-Champaign.

Competing interests statement

The authors declare that they have no competing financial interests.

Correspondence and requests for materials should be addressed to J.S.M. (e-mail: moore@scs.uiuc.edu).

Striped iron zoning of olivine induced by dislocation creep in deformed peridotites

J. Ando*, Y. Shibata*, Y. Okajima*, K. Kanagawa†, M. Furusho‡ & N. Tomioka§

* *Department of Earth and Planetary Systems Science, Hiroshima University, Higashi-Hiroshima 739-8526, Japan*
† *Department of Earth Sciences, Chiba University, Chiba 263-8522, Japan*
‡ *OYO Corporation, 10-20 Hamasaki Avenue, Hyogo-ku, Kobe 652-0807, Japan*
§ *Department of Earth and Planetary Sciences, Kobe University, Kobe 657-8501, Japan*

Deformation of solid materials affects not only their microstructures, but also their microchemistries[1–5]. Although chemical unmixing of initially homogeneous multicomponent solids is known to occur during deformation by diffusion creep[4,5], there has been no report on their chemical zoning due to deformation by dislocation creep, in either natural samples or laboratory experiments. Here we report striped iron zoning of olivine ($(Mg,Fe)_2SiO_4$) in deformed peridotites, where the iron concentration increases at subgrain boundaries composed of edge dislocations. We infer that this zoning is probably formed by alignment of edge dislocations dragging a so-called Cottrell 'atmosphere' of solute atoms[3,6,7] (iron in this case) into subgrain boundaries during deformation of the olivine by dislocation creep. We have found that the iron zoning does not develop in laboratory experiments of high strain rates where dislocations move too fast to drag the Cottrell atmosphere. This phenomenon might have important implications for the generation of deep-focus earthquakes, as transformation of olivine to high-pressure phases preferentially occurs in high-iron regions, and therefore along subgrain boundaries which would be preferentially aligned in plastically deformed mantle peridotites.

We have done microstructural and microchemical analyses of olivine grains in deformed mantle-derived peridotites from the Uenzaru peridotite complex in the Hidaka metamorphic belt of central Hokkaido, Japan. Olivine grains develop a lattice preferred orientation (LPO) characterized by a [100] density maximum subparallel to lineation, as commonly observed in deformed peridotites[8]. Most olivine grains in our samples exhibit undulose extinction or kink bands due respectively to gradual or sharp intragranular misorientation (Fig. 1). It is known that such microstructures are formed by alignment of dislocations into planar arrays to form subgrain boundaries due to crystal plastic deformation. Oxidation decoration[9] and subsequent observation by scanning electron microscopy[10] revealed that zones of undulose extinction in fact correspond to subgrain boundaries. In addition, transmission electron microscopy (TEM) revealed that subgrain boundaries are composed of edge dislocations with (010)[100] or {0*kl*}[100] slip, and that dislocation densities are high—of the order of 10^7–10^8 cm^{-2} (data not shown). These dislocation microstructures, as well as developed LPO, indicate that the olivine grains in our samples have been deformed by dislocation creep.

Striped zoning of Mg and in particular of Fe is easily visible in olivine grains that exhibit undulose extinction: the zoning is revealed by mapping of element concentrations using electron-probe microanalysis. The regions of low Mg and high Fe concentrations are exactly parallel to zones of undulose extinction—that is, subgrain boundaries (Fig. 2). Measurements of Fe concentration across subgrain boundaries by analytical transmission electron microscopy (ATEM) clearly indicate that Fe concentration increases at subgrain boundaries (Fig. 3). Areas of high Fe concentration correspond to those of low Mg concentration (Table 1), indicating that the striped zoning is formed via interdiffusion between Mg and

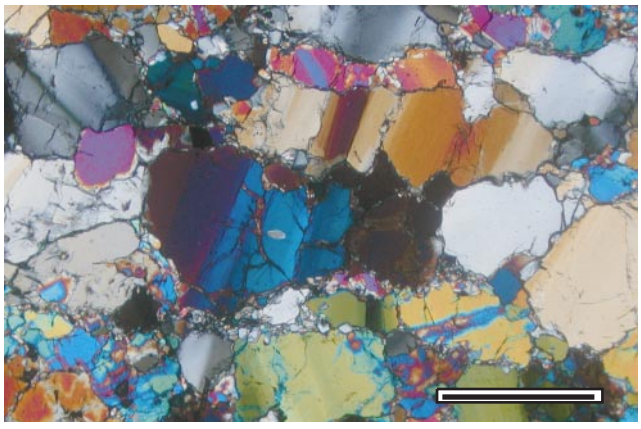

Figure 1 Optical micrograph in crossed polarized light, showing undulose extinction and kink bands (NNE–SSW direction) in olivine grains of an Uenzaru peridotite. Such olivine microstructures are commonly developed in deformed peridotites derived from the Earth's upper mantle. Scale bar, 1 mm.

Fe. Both electron-probe microanalysis and ATEM measurements indicate that the concentrations of fayalite (Fe_2SiO_4) components at subgrain boundaries are 1–1.5% higher than those in the other regions (Fig. 3 and Table 1). Such striped Fe zoning of olivine as described here is also found in deformed peridotites from the Horoman peridotite complex of the Hidaka metamorphic belt, as well as in those from the Baldissero, Balumuccia and Finero peridotite complexes in the Ivrea zone of the southern Alps. The striped Fe zoning of olivine may therefore be common in mantle peridotites.

Dislocation cores that give rise to elastic distortion of the crystal lattice attract solute atoms in alloys and minerals, forming Cottrell atmospheres[3,6,7]. Olivine is a solid solution between Mg_2SiO_4 (forsterite) and Fe_2SiO_4 (fayalite), in which Fe^{2+} is a solute cation. ATEM measurements[3] of X-ray intensities of Fe across a free edge dislocation in olivine from a mantle peridotite have revealed that Fe concentration increases in the immediate vicinity (less than 0.5 μm) of the dislocation, indicating a Cottrell atmosphere of solute Fe. During dislocation creep of a crystal, dislocation glide and climb enable dislocations to align in planar arrays and form subgrain boundaries such that the internal strain energy of the crystal is minimized. The formation of subgrain boundaries composed of edge dislocations dragging a Cottrell atmosphere of Fe can therefore produce a striped Fe zoning of olivine.

Two possible post-deformational processes may also affect the striped Fe zoning via pipe diffusion of Fe along dislocations: subsolidus reaction[11,12] and metasomatism[13]. The sources of Fe in these two cases are clinopyroxene and an Fe-rich fluid phase, respectively. However, the striped Fe zoning of olivine is developed even in dunite and harzburgite in which clinopyroxene is absent. In addition, Fe-enrichment at the rims of olivine grains possibly in direct contact with fluid was not detected. Laihunite, an Fe^{3+}-bearing olivine, has been reported to be formed as 0.6-nm-thick layer parallel to (001) along dislocation cores and grain boundaries of olivine during metasomatism of mantle peridotites under upper-mantle conditions[13,14]. But laihunite and any other precipitates were not found along subgrain boundaries by our TEM observations. An additional synchrotron micro-XANES study (not shown) did not detect Fe^{3+} in the iron-rich or in the iron-poor areas of the olivine grains that we studied (XANES; X-ray absorption near edge structure). The possibility of mantle metasomatism is therefore excluded, and consequently, post-deformational processes cannot be responsible for the observed striped Fe zoning of olivine.

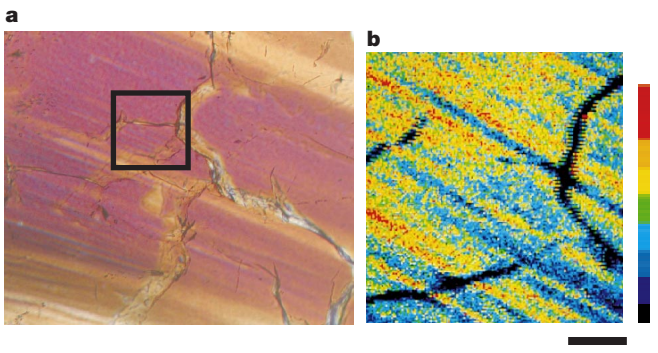

Figure 2 Microstructure and microchemistry of a strongly deformed olivine grain, indicating the relationship between undulose extinction and Fe zoning. **a**, Optical micrograph in crossed polarized light, showing undulose extinction in the WNW–ESE direction. **b**, Map of Fe concentrations within the rectangle shown in **a**. Striped Fe zoning in the WNW–ESE direction can be seen. Reddish colours indicate higher Fe concentrations (see colour bar on right of panel). Scale bar (black, at bottom), 30 μm. Black lines cutting the striped Fe zoning in **b** are cracks. Note that high-Fe areas are exactly parallel to zones of undulose extinction, that is, subgrain boundaries.

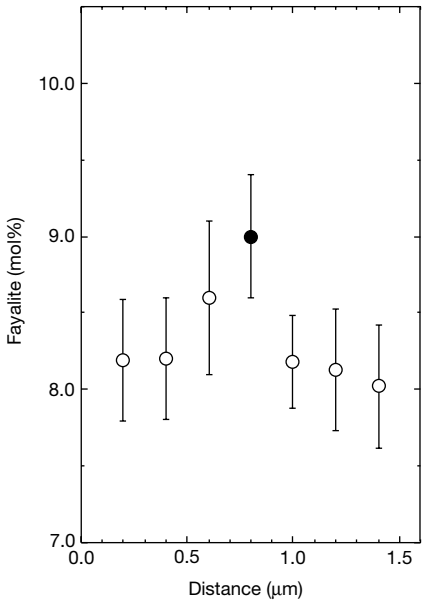

Figure 3 Fayalite (Fe_2SiO_4) components measured by ATEM across a subgrain boundary composed of edge dislocations. The filled circle shows a measurement made just at the subgrain boundary. The Fe concentration at the subgrain boundary is higher than that in the adjacent areas.

The (010)[100] and {0*kl*}[100] slip systems in olivine observed in the Uenzaru peridotites are active at relatively high temperatures—for example, at temperatures higher than 900 °C when the confining pressure and strain rate are 1,500 MPa and 10^{-4} s^{-1}, respectively[15]. Furusho and Kanagawa[16] have suggested that the Uenzaru peridotites are deformed at temperatures of 760–960 °C and pressures of 700–1,000 MPa. These ranges of temperatures and pressures correspond to those in the uppermost mantle and in descending slabs[17–19].

Subgrain boundaries composed of edge dislocations are perpendicular to the slip direction, that is, the Burgers vector. TEM observations (not shown) of dislocations in the studied olivine grains indicate the slip direction to be [100], and therefore subgrain boundaries are parallel to (100). In fact, optically visible subgrain boundaries in olivine grains are mostly parallel to their (100) planes.

Table 1 Chemical composition of olivine

	Fe-poor region			Fe-rich region		
SiO_2	40.91	40.90	41.09	40.77	40.48	40.94
TiO_2	0.02	—	—	0.01	0.02	0.02
FeO	8.35	8.00	7.66	9.22	9.14	8.92
NiO	0.33	0.40	0.37	0.34	0.36	0.36
Cr_2O_3	0.00	0.04	0.03	0.01	0.03	0.02
MnO	0.10	0.14	0.16	0.18	0.15	0.14
MgO	50.71	49.52	50.25	49.70	49.92	49.61
CaO	0.02	—	0.02	—	—	—
Total	100.44	99.00	99.58	100.23	100.10	100.01
No. of cations (O=4)						
Si	0.993	1.005	1.002	0.996	0.990	1.000
Ti	0.000	—	—	0.000	0.000	0.000
Fe	0.169	0.164	0.156	0.188	0.187	0.182
Ni	0.006	0.008	0.007	0.007	0.007	0.007
Cr	0.000	0.001	0.001	0.000	0.001	0.000
Mn	0.002	0.003	0.003	0.004	0.003	0.003
Mg	1.835	1.814	1.827	1.809	1.821	1.806
Ca	0.001	—	0.001	—	—	—
Total	3.006	2.995	2.997	3.004	3.009	2.998
Fa*	8.4	8.3	7.9	9.4	9.3	9.2

Compositions are given in wt%. Dash indicates under detection limit (<0.01 wt%). All measurements are within a single olivine grain. Fa* = 100 × Fe/(Mg + Fe).

LPO with a [100] density maximum close to lineation indicates preferred alignment of (100) and hence subgrain boundaries normal to lineation. This has an important implication for the generation of deep-focus earthquakes, which are possibly triggered by transformation of olivine to high-pressure phases[19–24]. In a descending slab, the phase transformation of olivine to β-phase (wadsleyite) and γ-phase (ringwoodite) would occur first at regions of high Fe concentrations, because Fe-rich olivine transforms at a lower pressure than Mg-rich olivine at the same temperatures[25,26]. Moreover, stacking faults along which the crystal lattice is transformed to ringwoodite are preferentially formed parallel to (100) in olivine[27,28]. Thus the phase transformation would preferentially occur parallel to (100) in olivine, which is preferentially aligned normal to lineation, that is, in planar arrays. The high-pressure phases thus formed are much finer-grained than the host olivine[21,23,24], and possibly deform superplastically by a grain-size-sensitive flow—in contrast to the host olivine plastically deforming by grain-size-insensitive dislocation creep. The formation of high-pressure phases in planar arrays may therefore lead to shear instability in descending slabs, and trigger deep-focus earthquakes in these slabs.

Orowan's equation indicates that strain rate is proportional to dislocation velocity[29]. The observed Fe zoning in naturally deformed olivine implies the moving of dislocations at speeds slow enough to drag a Cottrell atmosphere, probably because of very low strain rates ($\sim 10^{-14}\,s^{-1}$) in the mantle. If the strain rate is much higher, as in deformation experiments (generally $\geq 10^{-6}\,s^{-1}$), fast-moving dislocations would leave the Cottrell atmosphere behind, resulting in no Fe concentrations along dislocations. The presence of a Cottrell atmosphere also has a pinning effect on dislocations and inhibits their movement. Accordingly, flow laws at high and low strain-rate conditions are different[30]. Hence the plasticity of olivine at very low strain rates in the mantle may be different from that at the high strain rates achieved in the laboratory—this needs to be explored in the future, to obtain a better understanding of the dynamics of the Earth's interior. □

Received 23 August; accepted 6 November 2001.

1. Li, J. C. M., Nolfi, F. V. Jr & Johnson, C. A. Diffusional equilibrium of substitutional atoms in a stressed solid. *Acta Metall.* **19,** 749–752 (1971).
2. Green, H. W. II On the thermodynamics of non-hydrostatically stressed solids. *Phil. Mag.* **41,** 637–647 (1980).
3. Kitamura, M., Matsuda, H. & Morimoto, N. Direct observation of the Cottrell atmosphere in olivine. *Proc. Jpn Acad.* **62,** 149–152 (1986).
4. Dimos, D., Wolfenstine, J. & Kohlstedt, D. L. Kinetic demixing and decomposition of multi-component oxides due to a nonhydrostatic stress. *Acta Metall.* **36,** 1543–1552 (1988).
5. Ozawa, K. Stress-induced Al–Cr zoning of spinel in deformed peridotites. *Nature* **338,** 141–144 (1989).
6. Cottrell, A. H. in *Report of the Strength of Solids* 30–36 (The Physical Society, London, 1948).
7. Blavette, D., Cadel, E., Fraczkiewicz, A. & Menand, A. Three-dimensional atomic-scale imaging of impurity segregation to line defects. *Science* **286,** 2317–2319 (1999).
8. Ben Ismail, W. & Mainprice, D. An olivine fabric database: An overview of upper mantle fabrics and seismic anisotropy. *Tectonophysics* **296,** 145–157 (1998).
9. Kohlstedt, D. L., Goetze, C., Durham, W. B. & Vandersande, J. B. New technique for decorating dislocations in olivine. *Science* **19,** 1045–1091 (1976).
10. Karato, S. Scanning electron microscope observation of dislocations in olivine. *Phys. Chem. Minerals* **14,** 245–248 (1986).
11. Ozawa, K. Partitioning of elements between constituents minerals in peridotites from the Miyamori ultramafic complex, Kitakami Mountains, Northeast Japan: Estimation of P-T condition and igneous composition of minerals. *J. Fac. Sci. Univ. Tokyo II* **21,** 115–137 (1986).
12. Kawasaki, T & Ito, E. An experimental determination of the exchange of Fe^{2+} and Mg^{2+} between olivine and Ca-rich clinopyroxene. *Am. Mineral.* **79,** 461–477 (1994).
13. McGuire, A. V., Dyar, M. D. & Nielson, J. E. Metasomatic oxidation of upper mantle peridotite. *Contrib. Mineral. Petrol.* **109,** 252–264 (1991).
14. Banfield, J. F., Dyar, M. D. & McGuire, A. V. The defect microstructure of oxidized mantle olivine from Dish Hill, California. *Am. Mineral.* **77,** 977–986 (1992).
15. Carter, N. L. & Ave Lallemant, H. G. High temperature flow of dunite and peridotite. *Geol. Soc. Am. Bull.* **81,** 2181–2202 (1970).
16. Furusho, M. & Kanagawa, K. Transformation-induced strain localization in a lherzolite mylonite from the Hidaka metamorphic belt of central Hokkaido, Japan. *Tectonophysics* **313,** 411–432 (1999).
17. Ito, E. & Sato, H. in *High-Pressure Research: Application to Earth and Planetary Sciences* (eds Syono, Y. & Manghnani, H.) 257–262 (Terrapub/American Geophysical Union, Tokyo/Washington DC, 1992).
18. Iidaka, T. & Furukawa, Y. Double seismic zone for deep earthquakes in the Izu-Bonin subduction zone. *Science* **263,** 1116–1118 (1994).
19. Kirby, S. H., Stein, S., Okal, E. A. & Rubie, D. C. Metastable mantle phase transformations and deep earthquakes in subducting oceanic lithosphere. *Rev. Geophys.* **34,** 261–306 (1996).
20. Kirby, S. H. Localized polymorphic phase transformations in high-pressure faults and applications to the physical mechanism of deep earthquakes. *J. Geophys. Res.* **92,** 13789–13800 (1987).
21. Green, H. W. II & Burnley, P. C. A new self-organizing mechanism for deep-focus earthquakes. *Nature* **341,** 733–737 (1989).
22. Kirby, S., Durham, W. B. & Stern, L. A. Mantle phase changes and deep-earthquake faulting in subducting lithosphere. *Science* **252,** 216–225 (1991).
23. Burnley, P. C., Green, H. W. II & Prior, D. J. Faulting associated with the olivine to spinel transformation in Mg_2GeO_4 and its implications for deep focus earthquakes. *J. Geophys. Res.* **96,** 425–443 (1991).
24. Tingle, T. N., Green, H. W. II, Scholtz, C. H. & Koczynnski, T. A. The rheology of faults triggered by the olivine–spinel transformation in Mg_2GeO_4 and its implications for the mechanism of deep focus earthquakes. *J. Struct. Geol.* **15,** 1249–1256 (1993).
25. Katsura, T. & Ito, E. The system Mg_2SiO_4 – Fe_2SiO_4 at high pressure and temperatures: precise determination of stabilities of olivine, modified spinel, and spinel. *J. Geophys. Res.* **94,** 15663–15670 (1989).
26. Akaogi, M., Ito, E. & Navrotsky, A. Olivine-modified spinel-spinel transitions in the system Mg_2SiO_4 – Fe_2SiO_4 : calorimetric measurements, thermochemical calculation, and geophysical. *J. Geophys. Res.* **94,** 15671–15685 (1989).
27. Poirier, J.-P. in *Anelasticity in the Earth* (eds Stacey, F. D., Paterson, M. S. & Nicholas, A.) 113–117 (American Geophysical Union and Geological Society of America, Washington DC/Boulder, 1981).
28. Kerschhofer, L., Rubie, D. C., Sharp, T. G., McConnell, J. D. C. & Dupas-Bruzek, C. Kinetics of intracrystalline olivine–ringwoodite transformation. *Phys. Earth Planet. Inter.* **121,** 59–76 (2000).
29. Poirier, J.-P. in *Creep of Crystals* 62–63 (Cambridge Univ. Press, Cambridge, 1985).
30. Yoshinaga, H. in *Rheology of Solids and of the Earth* (eds Karato, S. & Toriumi, M.) 29–41 (Oxford Science Publications, New York, 1989).

Acknowledgements

We thank K. Ozawa for critical reading of the manuscript, H. Ishisako for making thin sections, Y. Takahashi for his contribution to the XANES study at the KEK photon factory in Tsukuba, Japan, and N. Abe for supplying the specimens from the southern Alps. This study was supported by JSPS (J.A.).

Competing interests statement

The authors declare that they have no competing financial interests.

Correspondence and requests for materials should be addressed to J.A. (e-mail: ando@letitbe.geol.sci.hiroshima-u.ac.jp).

Horses damp the spring in their step

Alan M. Wilson*, M. Polly McGuigan*, Anne Su† & Anton J. van den Bogert†

** Department of Veterinary Basic Sciences, The Royal Veterinary College, Hatfield, Herts AL9 7TA, UK*

† Department of Biomedical Engineering, Cleveland Clinic Foundation, 9500 Euclid Avenue, Cleveland, Ohio 44195, USA

The muscular work of galloping in horses is halved by storing and returning elastic strain energy in spring-like muscle–tendon units[1,2].These make the legs act like a child's pogo stick that is tuned to stretch and recoil at 2.5 strides per second. This mechanism is optimized by unique musculoskeletal adaptations: the digital flexor muscles have extremely short fibres and significant passive properties, whereas the tendons are very long and span several joints[3,4]. Length change occurs by a stretching of the spring-like digital flexor tendons rather than through energetically expensive length changes in the muscle[5]. Despite being apparently redundant for such a mechanism[5], the muscle fibres in the digital flexors are well developed. Here we show that the mechanical arrangement of the elastic leg permits it to vibrate at a higher frequency of 30–40 Hz that could cause fatigue damage to tendon and bone. Furthermore, we show that the digital flexor muscles have minimal ability to contribute to or regulate significantly the 2.5-Hz cycle of movement, but are ideally arranged to damp these high-frequency oscillations in the limb.

In a 500-kg horse, about 1,000 J of elastic energy are stored in the digital flexor tendons and suspensory ligament (interosseus muscle) of each leg in each stride[2,6]. This is achieved by gravitational and